Mem. Natl Inst. Polar Res., Spec. Issue, **49**, 256–280, 1994

THERMAL MODELING OF ICE CORES AND BOREHOLES VIA THE FINITE ELEMENT TECHNIQUE

Debendra K. DAS and S. Srikanta JOIS

Department of Mechanical Engineering,
University of Alaska Fairbanks,
Fairbanks, Alaska 99775-1710, U.S.A.

Abstract: An axisymmetric finite element computer program was developed to calculate heat transfer in cylindrical (*r-z*) geometry. The technique is applicable to steady-state and time-dependent problems and can handle convective, temperature-prescribed and heat-flux-prescribed boundary conditions. It employs the heat capacity method through the Dirac delta function to represent latent heat effect during freezing or thawing and computes movement of the phase front. A number of tests with different materials and boundary conditions were conducted to validate this code against heat transfer situations with and without phase change. The results showed good agreement with exact analytical and numerical solutions.

The model was then applied to determine temperature profiles in ice cores. Subsequent investigations were made to determine the rate of freezing in a borehole and the movement of the freeze front with time. Furthermore, results were generated for predicting complete freeze-up of the ice test well maintained by the Polar Ice Coring Office for a number of boundary conditions.

1. Introduction

The Polar Ice Coring Office (PICO), operated by the University of Alaska Fairbanks for the National Science Foundation, is charged with the development and operation of ice coring drills and augers for scientific research. Ice cores recovered by these devices from Greenland and Antarctica will provide a continuous environmental record of the past several centuries. Scientists are currently analyzing these cores and the gases trapped in their pores to determine what global climatic conditions were in the past. Recovering these cores from great depths in ice sheets without damage and contamination is the primary objective of PICO. A second goal is to collect subglacial samples from bedrock beneath the ice pack.

Environmental Consideration: Common to all deep ice sampling devices to date has been the use of thousands of gallons of drilling fluids, such as diesel fuels, trichloroethylene, fluorocarbons, etc., in a designated pristine environment. Because of environmental concerns and the fact that contamination of the core may interfere with chemical analysis of the ice and trapped gases, thereby leading to inaccurate results, the search for an alternative deep ice core drilling fluid continues. We are also aware that new protocols are under discussion that may prohibit the use of conventional drilling fluids or, if allowed, may require the fluids to be pumped out of wells and removed from polar regions–a very expensive alternative.

Hot-Water-Mechanical Drill: In response to these concerns, PICO has introduced a conceptual design for a hot-water-mechanical drill suitable for coring through thick ice

caps in less time with hot water as the drilling fluid. A very important factor in this design is to ensure that heat transmission from the hot water to the ice core does not severely damage the core by fracturing or melting. A complete description of such a thermo-mechanical drill of PICO design is described in DAS *et al.* (1992).

1.1. Analytical study

For this reason, in the first phase of this study analytical solutions were developed (DAS *et al.,* 1991a) to determine temperature distributions in cylindrical ice cores while they were subjected to different initial and boundary temperatures. The cores were analyzed by three models: (1) an infinite cylinder model; (2) a semi-infinite cylinder model; and (3) a finite cylinder model.

In the infinite cylinder model, only radial heat conduction was considered. In the semi-infinite model, heat flow is assumed radially and from one end of the ice core, *e.g.,* the bottom of the core before the core is broken and extracted. In the finite cylinder model heat conduction was assumed both radially and axially from both ends. Detailed derivation of these solutions and computer programs for all three models have been described by DAS *et al.* (1991b). Using these models we performed parametric studies to determine core sizes that are obtainable for different surface temperatures due to the presence of hot water in thermal-mechanical drills without jeopardizing the interior region of the cores due to excessive heat penetration. Furthermore, the temperature distribution in a core can be used by stress analysts to determine conditions that prevent fracture in cold ice due to thermal stresses. In a later section of this paper we have presented some temperature profile results from the analytical solutions and have compared them to the finite element solutions.

The analytical methods developed during the first phase were able to predict temperature profiles in ice cores. These profiles gave us information about the upper temperature limit of the hot water in contact with the core barrel. From this information one can control the water temperature and flow rate in order to avoid overheating the core. However, these analytical techniques were based on many simplifying assumptions which were not necessarily valid under actual field conditions. For example, for these theories to apply, a constant surface temperature around the core must prevail, which may not be a realistic boundary condition. Therefore, improvements in these modeling techniques were necessary and this led to development of a general finite element model that could overcome the limitations of the present analytical methods.

1.2. Finite element approach

The finite element program was developed in two steps. In the first step, an algorithm was developed that could solve axisymmetric heat conduction problems with variable thermal properties and boundary conditions, but without the capability of handling the phase change aspect of the problem that occurs in thawing and freezing media. Then this initial portion of the program was validated by comparing the computed results with available analytical and numerical solutions for steady and transient heat conduction problems. In the second stage, the phase change ability was incorporated into the theory using the Dirac delta function approach of O'NEILL (1983a,b). Since there are no exact analytical solutions available for complex phase change problems, the program was verified against numerical solutions and approximate integral solutions. Finally, the

program was applied to practical cases:
1) for determining temperature profiles in ice cores in the initial phase of heating; 2) for determining ice borehole freeze-up time; and 3) to obtain the time required for complete freezing of the PICO ice test well.

2. Mathematical Formulation (Nonphase-Change Case)

2.1. Governing equation and boundary conditions

The two-dimensional heat conduction equation in cylindrical coordinates with circular symmetry is:

$$\frac{1}{r}\frac{\partial}{\partial r}\left(K_r r \frac{\partial T}{\partial r}\right) + \frac{\partial}{\partial z}\left(K_z \frac{\partial T}{\partial z}\right) + g - C\frac{\partial T}{\partial t} = 0. \tag{1}$$

Consider the two-dimensional region Ω with a total boundary Γ. The boundary conditions, in the most general form, are

$$K_r \frac{\partial T}{\partial r} n_r + K_z \frac{\partial T}{\partial z} n_z + h\,(T - T_\infty) + \hat{q} = 0, \qquad \text{on } \Gamma_1,\ t \geq 0 \tag{2}$$

$$T = \hat{T} \qquad \text{on } \Gamma_2,\ t \geq 0 \tag{2a}$$

and the initial condition is

$$T = T_i. \qquad \text{in } \Omega \qquad \text{at } t = 0 \tag{2b}$$

2.2. Semidiscrete variational formulation

The semidiscrete variational formulation of eqs. (1) and (2) following REDDY (1984) can be found by multiplying the equations with a test function v and integrating them over a typical element $\Omega^{(e)}$ with the application of the divergence theorem.

$$\int_{\Omega^{(e)}} \left(K_r r \frac{\partial v}{\partial r}\frac{\partial T}{\partial r} + K_z r \frac{\partial v}{\partial z}\frac{\partial T}{\partial z} - vrg + Cvr\frac{\partial T}{\partial t}\right) dr\,dz + \oint_{\Gamma^{(e)}} \{ rvh\,(T - T_\infty) + rv\hat{q} \}\,ds = 0. \tag{3}$$

The finite-element interpolation of the primary variable (temperature) is separated into spatial and time coordinates.

$$T(r, z, t) = \sum_{j=1}^{n} T_j(t)\,\Psi_j(r, z). \tag{4}$$

Substituting eq. (4) and $v = \Psi_i$ into eq. (3), we obtain the matrix equation

$$[M^{(e)}]\{\dot{T}\} + [K^{(e)}]\{T\} = \{F^{(e)}\}, \tag{5}$$

where

$$K_{ij}^{(e)} = \int_{\Omega^{(e)}} \left(K_r r \frac{\partial \Psi_i}{\partial r} \frac{\partial \Psi_j}{\partial r} + K_z r \frac{\partial \Psi_i}{\partial z} \frac{\partial \Psi_j}{\partial z}\right) dr\, dz + \oint_{r^{(e)}} hr\, \Psi_i \Psi_j\, ds$$

$$= K_{kij}^{(e)} + H_{ij}^{(e)}, \tag{6a}$$

$$M_{ij}^{(e)} = \int_{\Omega^{(e)}} Cr \Psi_i \Psi_j\, dr\, dz, \tag{6b}$$

$$F_i^{(e)} = \oint_{\Gamma^{(e)}} r(hT_\infty - \hat{q})\, \Psi_i\, ds + \int_{\Omega^{(e)}} \Psi_i r g\, dr\, dz \tag{6c}$$

$$= F_{ci}^{(e)} - F_{qi}^{(e)} + F_{gi}^{(e)}.$$

The simplest element for a general axisymmetric problem is an axisymmetric ring generated by a triangle revolved around the z-axis as illustrated in HUEBNER and THORNTON (1982). For triangular elements, the shape functions can be expressed in terms of area coordinates for which exact formulas are available in REDDY (1984) for integration over line path and the area. A linear interpolation function for the triangular element is assumed.

$$\Psi_i^{(e)} = \frac{1}{2A_e}(\alpha_i + \beta_i r + \gamma_i z); \qquad i = 1, 2, 3 \tag{7}$$

where α_i, β_i, γ_i are constants for a given element and are given by

$$\alpha_i = r_j z_k - r_k z_j; \qquad \beta_i = z_j - z_k; \qquad \gamma_i = r_k - r_j. \tag{8}$$

After substituting eqs. (7) and (8) into eq. (6) and evaluating the line and area integrals, with the help of closed form expressions available from REDDY (1984) and SQUARE (1970), the following matrices for each element were obtained.

$$[M^{(e)}]\{\dot{T}\} + ([K_k^{(e)}] + [H^{(e)}])\{T\} = \{F_c^{(e)} - F_q^{(e)}\} + \{F_g^{(e)}\}, \tag{9}$$

where

$$[M_{ij}^{(e)}] = \frac{C}{4A_e^2}\Bigg[(\alpha_i \alpha_j A_e \bar{r} + \alpha_i \beta_j + \beta_i \alpha_j)\frac{A_e}{12}\left(\sum_{i=1}^{3} r_i^2 + 9\bar{r}^2\right) +$$

$$(\alpha_i \gamma_j + \gamma_i \alpha_j)\frac{A_e}{12}\left(\sum_{i=1}^{3} r_i z_i + 9\bar{r}\bar{z}\right) + \beta_i \beta_j \frac{A_e}{12}\left(\sum_{i=1}^{3} r_i^3 + 9\bar{r}^3\right) + \tag{9a}$$

$$(\beta_i \gamma_j + \gamma_i \beta_j)\frac{A_e}{12}\left(\sum_{i=1}^{3} r_i^2 z_i + 9\bar{r}^2\bar{z}\right) + \gamma_i \gamma_j \frac{A_e}{12}\left(\sum_{i=1}^{3} r_i z^2 + 9\bar{r}\bar{z}^2\right)\Bigg]$$

$$\bar{r} = (r_1 + r_2 + r_3)/3, \quad \bar{z} = (z_1 + z_2 + z_3)/3,$$

$$[K_{kij}^{(e)}] = \frac{\bar{r}}{4A_e}[K_r \beta_i \beta_j + K_z \gamma_i \gamma_j]; \qquad i \text{ and } j = 1, 2, 3, \tag{9b}$$

$$[H^{(e)}] = \frac{hl_{12}}{12}\begin{bmatrix} 3r_1+r_2 & r_1+r_2 & 0 \\ r_1+r_2 & r_1+3r_2 & 0 \\ 0 & 0 & 0 \end{bmatrix} + \frac{hl_{23}}{12}\begin{bmatrix} 0 & 0 & 0 \\ 0 & 3r_2+r_3 & r_2+r_3 \\ 0 & r_2+r_3 & 3r_3+r_2 \end{bmatrix} + \frac{hl_{31}}{12}\begin{bmatrix} 3r_1+r_3 & 0 & r_1+r_3 \\ 0 & 0 & 0 \\ r_1+r_3 & 0 & r_1+3r_3 \end{bmatrix}, \tag{9c}$$

$$\{F_c^{(e)} - F_q^{(e)}\} = \frac{(hT_\infty - \hat{q})\, l_{12}}{6}\begin{bmatrix} 2r_1+r_2 \\ r_1+2r_2 \\ 0 \end{bmatrix} + \frac{(hT_\infty - \hat{q})\, l_{23}}{6}\begin{bmatrix} 0 \\ 2r_2+r_3 \\ r_2+2r_3 \end{bmatrix} + \frac{(hT_\infty - \hat{q})\, l_{31}}{6}\begin{bmatrix} 2r_1+r_3 \\ 0 \\ r_1+2r_3 \end{bmatrix}, \tag{9d}$$

$$\{F_g^{(e)}\} = \frac{g}{2}\left[\alpha_i \bar{r} + \frac{\beta_i}{12}\left(\sum_{i=1}^{3} r_i^2 + 9\bar{r}^2\right) + \frac{\gamma_i}{12}\left(\sum_{i=1}^{3} r_i z_i + 9\bar{r}\bar{z}\right)\right]. \tag{9e}$$

These expressions are given in detail here instead of the compact matrix form found in text books so that a potential user can program these expressions directly into a computational algorithm.

3. Addition of Phase Change Capability

The ability to handle phase change was incorporated into the mathematical formulation by introducing the Dirac delta function in the heat capacity, as demonstrated successfully by O'NEILL (1983a,b). The heat capacity is expressed in terms of the latent heat and the Dirac delta function as

$$C_{\text{eff}} = C + L\,\delta\,(T - T_o). \tag{10}$$

It is evident from eq. (6b) that the only matrix to be affected by inclusion of the latent heat term is the heat capacity matrix. The new heat capacity matrix equation is now

$$M_{ij}^{(e)} = \int_{\Omega^{(e)}} Cr\,\Psi_i \Psi_j \,dr\,dz + L \int_{\Omega^{(e)}} r\delta\,(T - T_o)\,\Psi_i\,\Psi_j \,dr\,dz. \tag{11}$$

For elements that do not contain the phase change isotherm, the second term in eq. (11), called the latent heat integral (*LHI*), becomes zero and the constant heat capacity term is evaluated in exactly the same fashion as the problem without phase change.

To apply the property of the Dirac delta function in the evaluation of *LHI*, it was reformulated in terms of a local coordinate system (σ-τ), as shown in Fig.1, within an element that is undergoing phase change. This technique has been used successfully by GOERING (1984) and SRIVASTAVA (1988). In linear triangular elements, the phase change isotherm is linear and the τ-axis is along and the σ-axis is perpendicular to this isotherm. The latent heat integral in terms of the new coordinates becomes

$$LHI = L \int_{\Omega^{(e)}} r\delta\,(T - T_o)\,\Psi'_i \Psi'_j \,d\sigma\,d\tau, \tag{12}$$

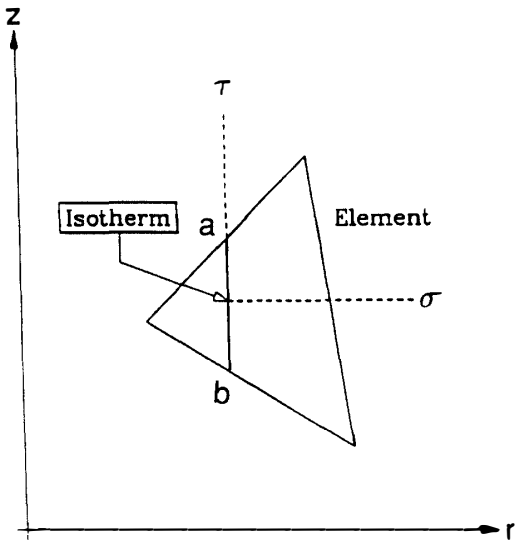

Fig. 1. A typical element showing the local coordinate system and the phase change isotherm that separates the thawed and frozen region.

where Ψ_i and Ψ'_j are the new shape functions in terms of local coordinates and are written as

$$\Psi'_i = \frac{(\Psi_{ib} - \Psi_{ia})}{l}\tau + \Psi_{ia} \quad ; \quad \Psi'_j = \frac{(\Psi_{jb} - \Psi_{ja})}{l}\tau + \Psi_{ja}. \qquad (13a, b)$$

Rewriting the integral in eq. (12) by introducing a temperature gradient term following O'NEILL (1983a, b),

$$LHI = L\int_{\Omega^{(e)}} r\delta\,(T-T_o)\,dT\,\Psi'_i\,\Psi'_j\frac{d\sigma}{d\tau}\,d\tau. \qquad (14)$$

The benefit of this transformation is apparent by recognizing that a mathematical property of the Dirac delta function integral with temperature terms is equal to unity. Therefore, the integral in eq. (14) simplifies to

$$LHI = L\int_{\Omega^{(e)}} r\Psi'_i\Psi'_j\frac{d\sigma}{dT}\,d\tau. \qquad (15)$$

As the temperature gradient is perpendicular to the phase change isotherm, it is also parallel to the σ-axis. The temperature gradients are also constant within each element for a linear triangular element. The inverse of the gradient in integral (15) represents magnitude of the temperature gradient, which can be written as

$$\frac{d\sigma}{dT} = \frac{1}{|\nabla T|}. \qquad (16)$$

The general expression for temperature gradient within an element is

$$|\nabla T| = \frac{1}{2A_e}\left(\sqrt{(T_1\beta_1 + T_2\beta_2 + T_3\beta_3)^2 + (T_1\gamma_1 + T_2\gamma_2 + T_3\gamma_3)^2}\right). \qquad (17)$$

Substituting the inverse of temperature gradient in the integral of eq. (15), we obtain

$$LHI = L \frac{1}{|\nabla T|} \int r \Psi'_i \Psi'_j d\tau . \tag{18}$$

The radial coordinate r is now expressed in terms of the shape functions, which are based on the new local coordinate (σ, τ) system.

$$r = r_1 \Psi'_1 + r_2 \Psi'_2 + r_3 \Psi'_3 . \tag{19}$$

When expressions for the radial coordinate and modified shape functions are introduced into eq. (18), we find the following integral.

$$M^l_{ij} = L \frac{1}{|\nabla T|} \int_o^l (r_1 \Psi'_1 + r_2 \Psi'_2 + r_3 \Psi'_3) \left\{ \left(\frac{\Psi_{ib} - \Psi_{ia}}{l} \right) \tau + \Psi_{ia} \right\} \left\{ \left(\frac{\Psi_{jb} - \Psi_{ja}}{l} \right) \tau + \Psi_{ja} \right\} d\tau. \tag{20}$$

This integral (20) represents latent heat effect for the ij^{th} term in the element heat capacity matrix. The integral is evaluated within limits 0 to l and results in lengthy integrations. Fortunately, they yield exact analytical results without requiring any numerical integration. After the necessary algebra, we have obtained an analytic expression for the ij^{th} term of the latent heat matrix. Since this important final expression was not cited in the literature anywhere, we have listed the complete expression here for use by potential users.

$$M^l_{ij} = L \frac{1}{|\nabla T|} \left(\frac{C_1 l^4}{4} + \frac{C_2 l^3}{3} + \frac{C_3 l^2}{2} + C_4 l \right), \tag{21}$$

where C_1, C_2, C_3, and C_4 are constants for any given element and are expressed as

$$C_1 = \frac{(\Psi_{ib} - \Psi_{ia})}{l} \frac{(\Psi_{jb} - \Psi_{ja})}{l} \left\{ r_1 \frac{(\Psi_{1b} - \Psi_{1a})}{l} + r_2 \frac{(\Psi_{2b} - \Psi_{2a})}{l} + r_3 \frac{(\Psi_{3b} - \Psi_{3a})}{l} \right\}, \tag{21a}$$

$$\begin{aligned} C_2 = \frac{1}{l^2} \Big[& (\Psi_{ib} - \Psi_{ia}) (\Psi_{jb} - \Psi_{ja}) (r_1 \Psi_{1a} + r_2 \Psi_{2a} + r_3 \Psi_{3a}) + \\ & \{ \Psi_{ia} (\Psi_{jb} - \Psi_{ja}) + \Psi_{ja} (\Psi_{ib} - \Psi_{ia}) \} \\ & \{ r_1 (\Psi_{1b} - \Psi_{1a}) + r_2 (\Psi_{2b} - \Psi_{2a}) + r_3 (\Psi_{3b} - \Psi_{3a}) \} \Big], \end{aligned} \tag{21b}$$

$$\begin{aligned} C_3 = \frac{1}{l} \Big[& \{ \Psi_{ja} (\Psi_{ib} - \Psi_{ia}) + \Psi_{ia} (\Psi_{jb} - \Psi_{ja}) \} (r_1 \Psi_{1a} + r_2 \Psi_{2a} + r_3 \Psi_{3a}) + \\ & \Psi_{ia} \Psi_{ja} \{ (r_1 (\Psi_{1b} - \Psi_{1a}) + r_2 (\Psi_{2b} - \Psi_{2a}) + r_3 (\Psi_{3b} - \Psi_{3a}) \} \Big], \end{aligned} \tag{21c}$$

$$C_4 = \Psi_{ia} \Psi_{ja} (r_1 \Psi_{1a} + r_2 \Psi_{2a} + r_3 \Psi_{3a}) . \tag{21d}$$

3.1. Thermal properties of partially frozen and partially thawed elements

In our computational steps, all elements are checked for their state. If the element is either completely frozen or completely thawed, then the respective thermal properties are assigned to the element. In case the element is undergoing phase change, it must contain the phase change isotherm within; therefore, the equivalent properties are calculated based

on the ratio of volume thawed (or volume frozen) to the total volume of the element. The thermal properties of such elements are based on the following equations.

$$\frac{1}{K_{eq}} = \frac{1}{K_f}\frac{V_f}{V_e} + \frac{1}{K_t}\frac{V_t}{V_e}. \tag{22a}$$

Inserting the expressions of volumes in axisymmetric ring elements one obtains

$$\frac{1}{K_{eq}} = \frac{1}{K_f}\frac{2\pi\bar{r}'A_f}{2\pi\bar{r}A_e} + \frac{1}{K_t}\frac{2\pi\bar{r}''A_t}{2\pi\bar{r}A_e}, \tag{22b}$$

where A_f and At are frozen and thawed portion of the total area A_e shown in Fig.1. The volumetric heat capacity relation is

$$C_{eq} = C_f\frac{V_f}{V_e} + C_f\frac{V_t}{V_e}. \tag{22c}$$

Here, V_e is the volume of the entire element, V_f is the volume of the frozen element, and V_t is the volume of the thawed element. Furthermore, $\bar{r}'$ is the centroid of the frozen portion of the element, $\bar{r}''$ is the centroid of the thawed portion of the element, and $\bar{r}$ is the centroid of the entire element. However, for simplicity the following approximate formulas may be used assuming $\bar{r}$, $\bar{r}'$, and $\bar{r}''$ are close to one another, which will be the case for small triangular elements.

$$\frac{1}{K_{eq}} = \frac{1}{K_t}\frac{A_t}{A_e} + \frac{1}{K_f}\frac{A_f}{A_e}\,;\; C_{eq} = C_t\frac{A_t}{A_e} + C_f\frac{A_f}{A_e}. \tag{23a, b}$$

3.2. Time-stepping scheme

For transient problems we have done the time descretization with the Θ method of approximation described in REDDY (1984). The temperature field at the end of a time step $\Delta t = t_{n+1} - t_n$ is obtained from the following equation.

$$\left([M] + \Theta\Delta t[K]\right)\{T\}_{n+1} = \left[[M] - (1-\Theta)\,\Delta t[K]\right]\{T\}_n + \Delta t\left[\Theta\,\{F\}_{n+1} + (1-\Theta)\{F\}_n\right]. \tag{24}$$

In the above equation, M and K represent the heat capacity and the conductivity matrix, as denoted earlier. Furthermore, F and T represent the heat load vector and temperature and $\{F\}_n$ and $\{T\}_{n+1}$ refer to the parameters at times t_n and t_{n+1} respectively. The well-known parameter Θ can have several values: 0 for the forward difference scheme, 1/2 for the Crank-Nicolson scheme, 2/3 for the Galerkin scheme, and 1 for the backward difference scheme. Both the Crank-Nicolson and the Galerkin schemes are unconditionally stable. We tried both of them for several test cases, and no significant difference in the final results were observed. Finally, we adopted the Crank-Nicolson scheme because of its wide usage and set $\Theta = 1/2$ in all of our subsequent runs.

We have developed the theory and the computational technique for our axisymmetric program following the two-dimensional cartesian program FEM2D of REDDY (1984). Further details on input, output, and running of the program, which we have named FEMRZ(Finite Element Model in *r-z* coordinates) can be found in SRIVASTAVA (1988) and JOIS (1992). In addition to ice drilling problems, this program has also been applied

successfully to predict dissociation of natural gas hydrates, which has been described by DAS and SRIVASTAVA (1991).

4. Validation (Nonphase-Change Cases)

4.1. Steady-state heat conduction examples

Case 1: An infinitely long, hollow cylinder of inner radius 1 m and outer radius 2 m is considered. Temperatures at the inner and outer surfaces are prescribed as 1000°C and 0°C, respectively. With forty elements and forty-two nodes, as shown in Fig. 2a, this problem was solved by the present finite element method. Our computed results match exactly with the analytical and numerical solutions presented by RAO (1989) for this problem, as seen from Fig. 2b.

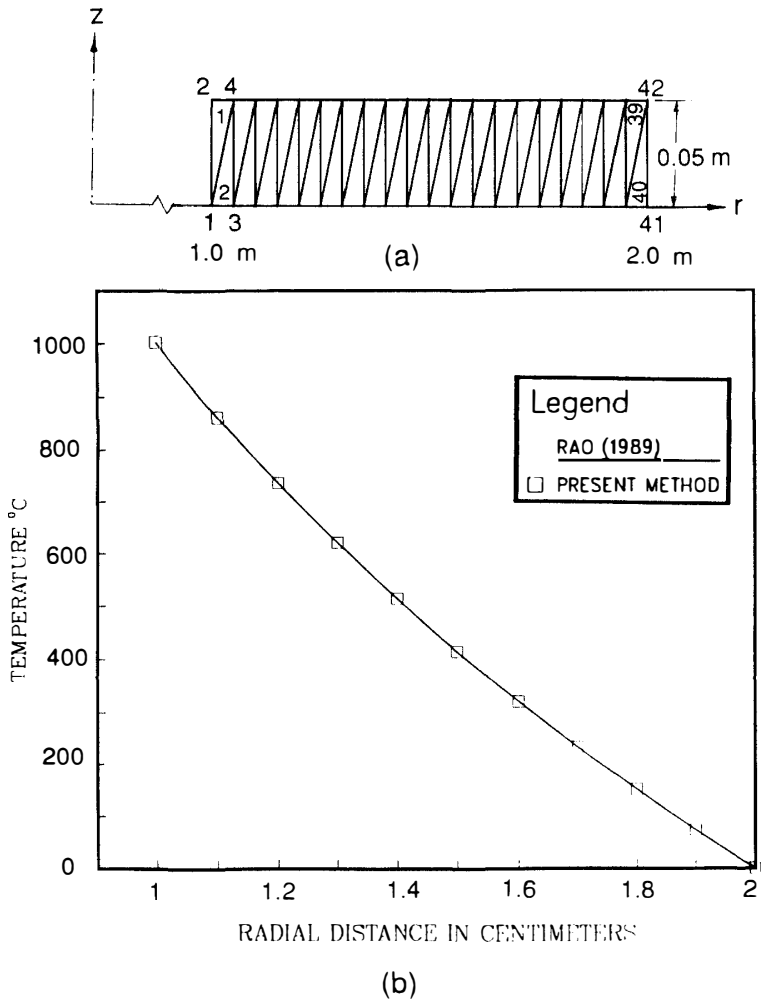

Fig. 2. (a) Mesh used to simulate the radial heat conduction problem in RAO (1989).
(b) Comparison between the solution given in RAO (1989) and the present finite element results.

Case 2: This problem consists of heat flow in a composite cylinder comprised of two media (Fig. 3a) as presented by HUEBNER and THORNTON (1982). The inner surface of the cylinder is held at $T = 200°C$, while the outer surface of low conductivity insulation is held

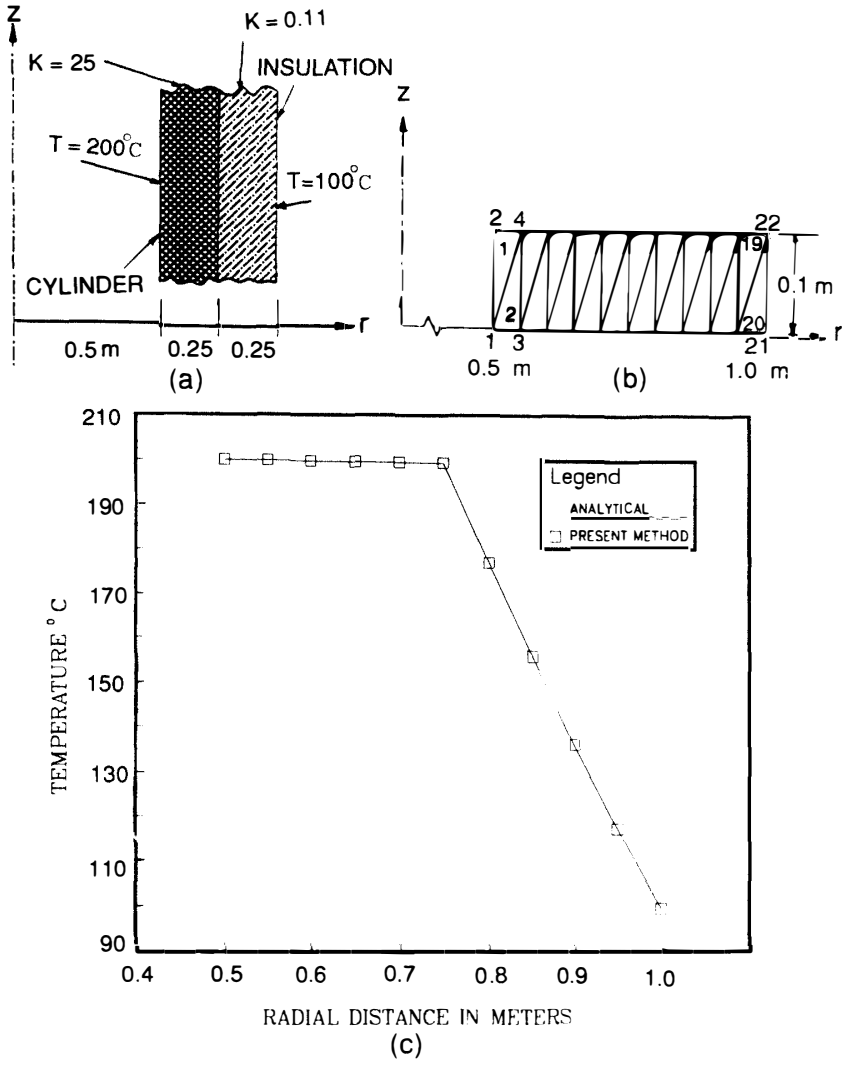

Fig. 3. (a) Geometry of the insulated hollow cylinder from HUEBNER *and* THORNTON *(1982). Thermal conductivity K in W/m·°C.*
(b) Mesh used to solve the problem in HUEBNER *and* THORNTON *(1982).*
(c) Comparison between the solution given in HUEBNER *and* THORNTON *(1982) and the present finite element solution.*

at $T = 100°C$. This problem was simulated with twenty elements and twenty-two nodes as shown in Fig. 3b. As evident from Fig. 3c, the finite element solution exactly matches the analytical and numerical solutions given in HUEBNER and THORNTON (1982).

4.2. Transient heat conduction examples

Case 3: This transient heat transfer problem with convective boundary condition has been taken from WHITE (1984). A short cylinder 16 cm high with a diameter of 6 cm is initially at 40°C and is then plunged into a fluid with $h = 300$ W/m$^2 \cdot$ K and an ambient temperature of 200°C. The material is bronze with a conductivity of 26 W/m · K and diffusivity of 8.6 (10^{-6}) m^2/s.

Because of symmetry about r-and z-axes, only one-quarter of the cylinder is modeled.

Two different types of mesh were used to ascertain that results would not change by changing mesh orientation (Figs. 4a and 4b): a) standard skew mesh, and b) reverse skew mesh. Both gave the same results and comparison of temperature at the center of the cylinder versus time in Fig. 4c shows a good agreement between analytical results from White and our finite element results. The analytical solution was obtained on the centerline using Heisler centerline formulas given by WHITE (1984).

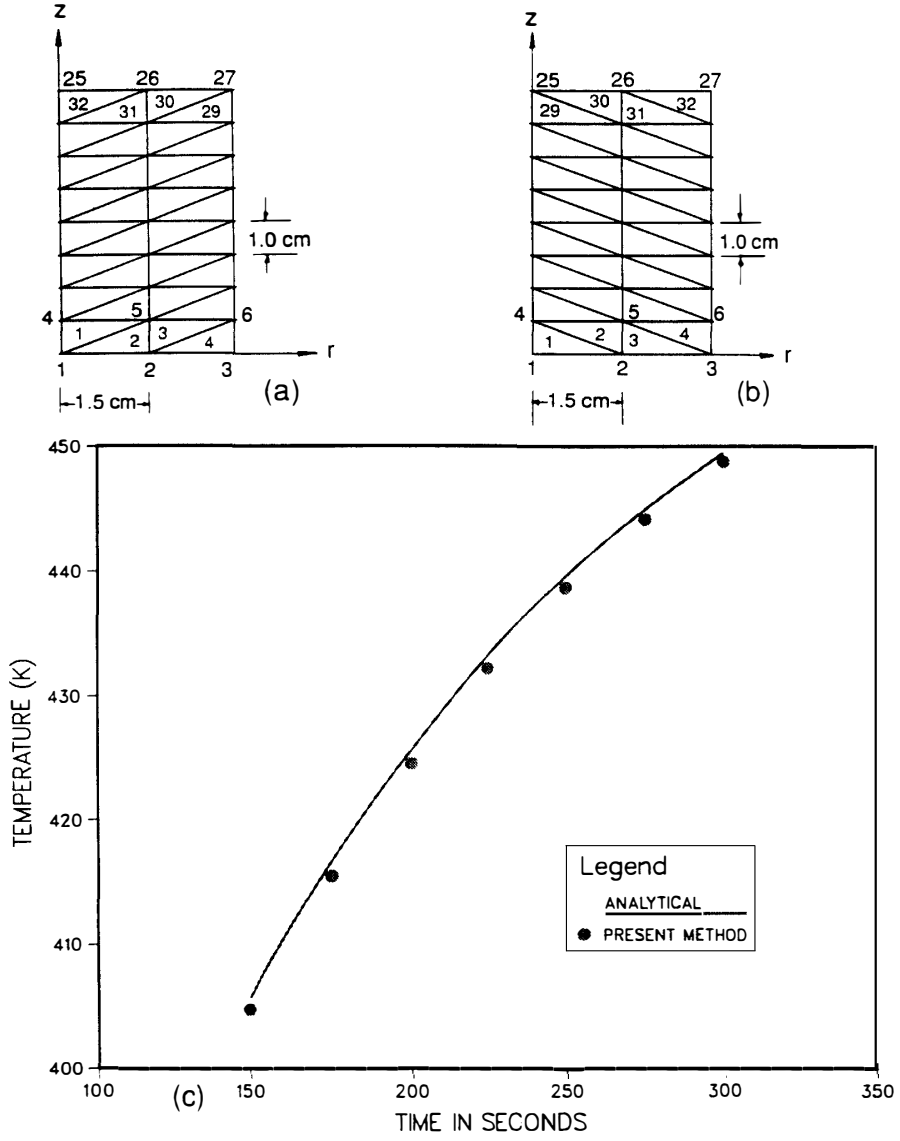

Fig. 4. (a) Mesh with a standard skewness to model the problem in WHITE (1984).
(b) Mesh with a reverse skewness to verify mesh independence.
(c) Comparison of temperature rise with time at the center of the cylinder by the present method and the solution in WHITE (1984).

Case 4: A 10 cm diameter, 16 cm long cylinder with conductivity 0.5 W/m·K and a diffusivity of $5(10^{-7})$ m^2/s is initially at a uniform temperature of 20°C. Suddenly, it was placed in hot air at 500°C and a convective coefficient of 30 W/m^2·K. Because of symmetry about r-and z-axes, only one-quarter of the cylinder is considered. As we did

for Case 3, to test mesh dependence, two different types of meshes were used based on standard and opposite skewness (Figs. 5a and 5b). The radial temperature profiles at the top (z=0) and at the center (z=8 cm) of the cylinder after thirty minutes of heating are compared with the analytical solution of KRIETH and BOHN (1986) in Fig. 5c. Both profiles show excellent agreement with the analytical solutions and demonstrate that changing skewness has minimal effect on this program.

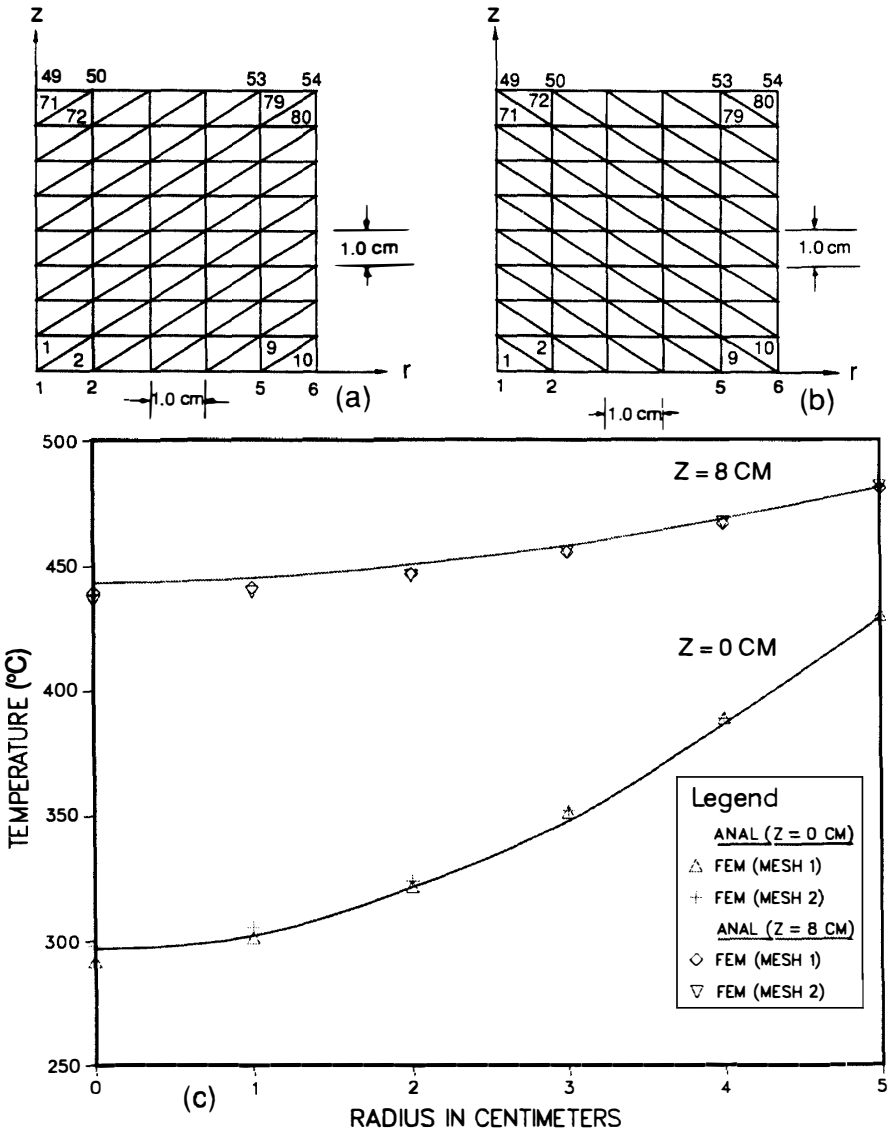

Fig. 5. (a) Mesh 1 with standard skewness to model the problem in KREITH and BOHN (1986).
(b) Mesh 2 with reverse skewness to verify mesh independence.
(c) Comparison of radial temperature distributions at the top and center of the cylinder after 30 minutes of heating via the present finite element method (FEM) and the analytical solutions from KREITH and BOHN (1986).

4.3. Validation of the method for phase change cases

Case 5: This problem of thawing around a circular pipe from LUNARDINI (1981) is an excellent source of comparison between four different solutions of a cylindrical phase

change problem as shown in Figs. 6a and 6b. The problem is tested with a radially varying mesh of 18 elements and 20 nodes for two values of superheat factor ϕ. The results of Sparrow, and Tien and Churchill, adapted from Lunardini and shown in Fig. 6b, are from numerical solutions. On the same figure, curves of approximate analytical solutions from the method of Lunardini, and the heat balance integral (HBI) method are also displayed. The analytical methods are described in detail in LUNARDINI (1981). Our finite element results show good agreement with all four methods, as observed in Fig. 6b.

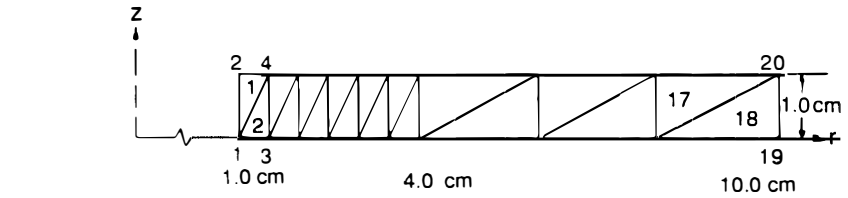

(a)

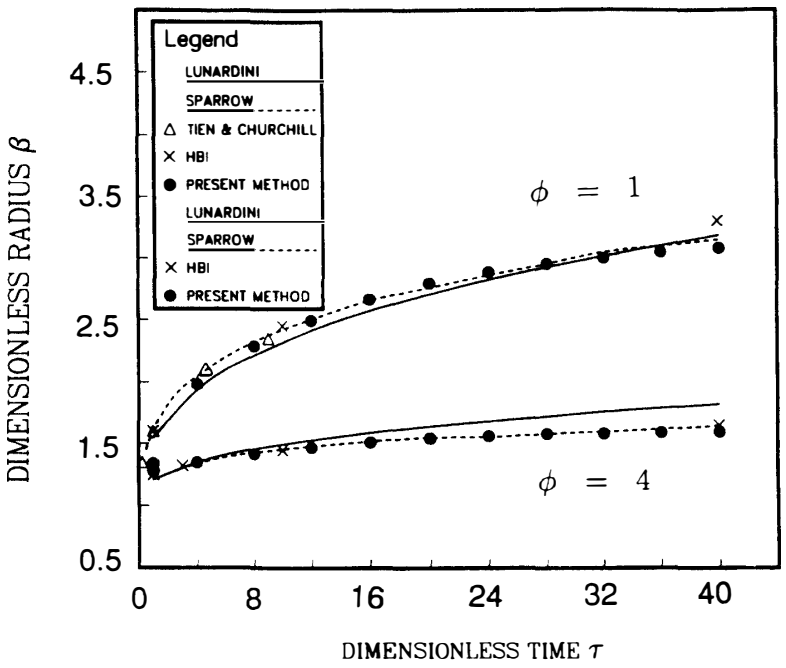

(b)

Fig. 6 (a) Mesh used for computation of thawing around a circular pipe from LUNARDINI (1981). (b) Comparison of four different methods from LUNARDINI (1981) with the present finite element method.

Case 6: This problem of radial freezing of water-saturated sand was taken from O'NEILL (1983a). It consists of outward radial freezing around an infinitely long hollow cylinder with time-dependent boundary conditions. The histories of boundary temperatures are presented by O'NEILL (1983a), which we inserted into our program by a polynomial as a function of time. The physical properties used for water-saturated sand and the mesh (324 elements, 196 nodes) used to simulate the problem are shown in JOIS (1992). The program was run for 100000 (27 hours) and the freeze-front radius presented in Fig. 7 was found to

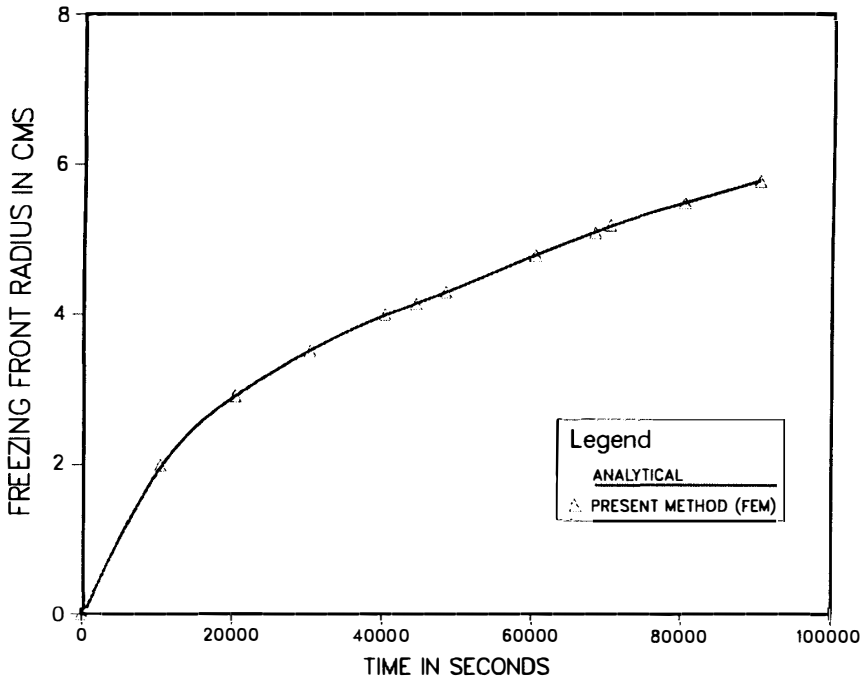

Fig. 7. Comparison of radial freezing in water-saturated sand between the results presented by O'NEILL (1983a) and the present finite element method.

be in good agreement with the analytical solution presented by O'NEILL (1983a).

5. Applications

5.1. Prediction of temperature profiles in ice cores

In hot-water ice coring, the thermal shock caused by warm water coming in contact with cold ice can result in thermally-induced stresses which can cause cracking of the cores. To determine these stresses, one must find the transient temperature profiles.

This example presents such a case for a finite ice cylinder undergoing transient heat conduction. This transient axisymmetric heat conduction problem yields to an analytical solution described in DAS *et al.* (1991a) expressed in a non-dimensional form. A similar solution is also reported by MYERS (1987) in a dimensional form. A short cylindrical ice core of 20 cm in diameter and 50 cm in length is considered whose geometry is shown in Fig. 8a. Because of the symmetry about r- and z-axes, only one-quarter of the cylinder (25 cm height × 10 cm width) is considered for simulation of this problem. The ice cylinder is initially maintained at a temperature of −40°C. The lateral and the circumferential surfaces of the cylinder are maintained at 0°C. The thermal diffusivity of ice is taken as 1.33×10^{-6} m^2/s. The mesh used to simulate the problem consists of 200 elements and 121 nodes, as displayed in Fig. 8b. The sides representing symmetry in Fig. 8b are considered insulated. Two comparisons (Figs. 8c and 8d) were made for several temperature profiles: the first one for different axial positions at time t = 1000 s, and the second one for different non-dimensionalized times at a fixed axial location of Z = 0.5 (mid-section of the cylinder). As seen from these plots, the finite element solutions match accurately with the analytical

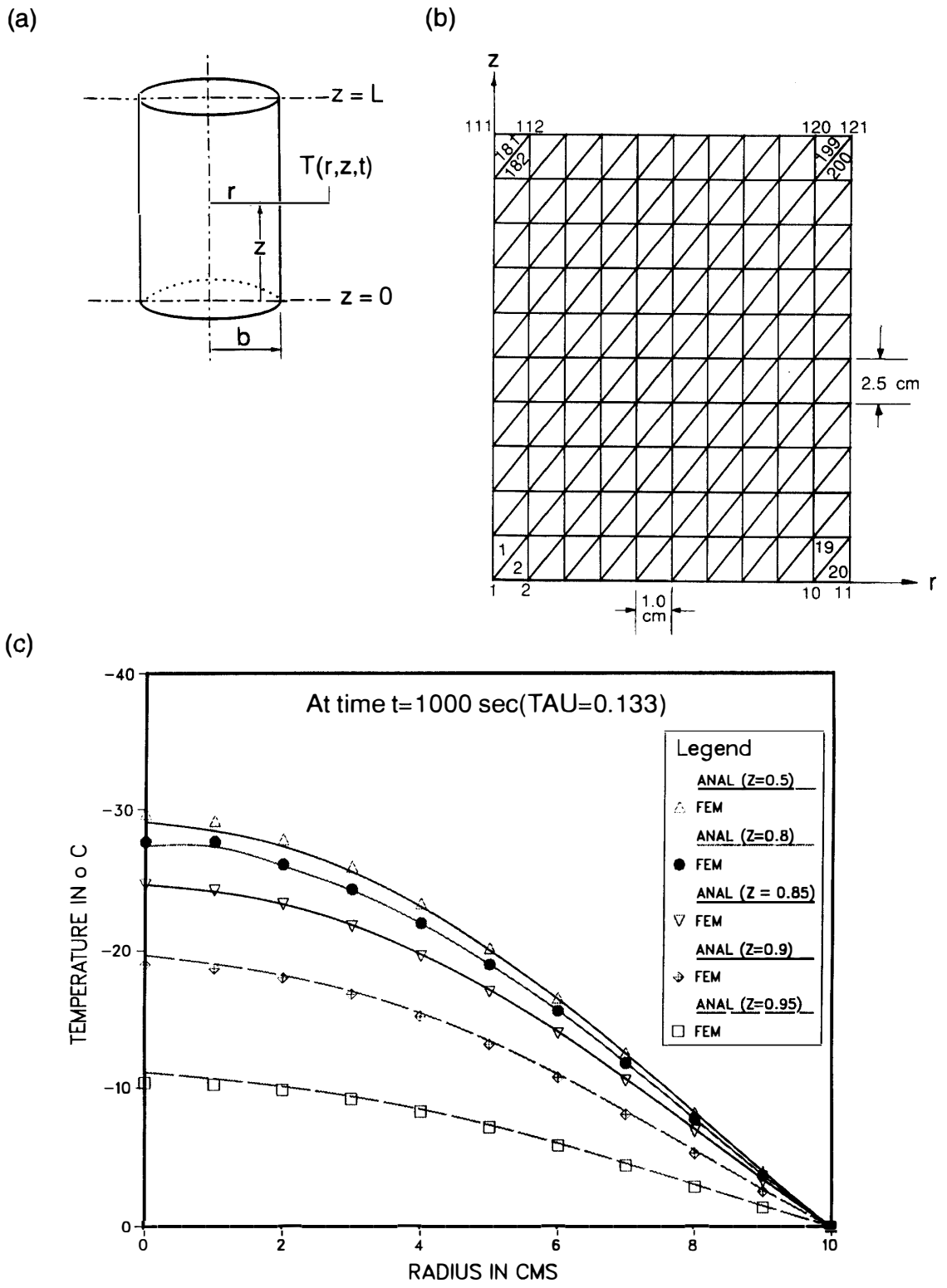

Fig. 8. *(a) Geometry of a finite cylindrical ice core.*
(b) Mesh used to simulate the heat conduction problem in a cylindrical ice core.
(c) Comparison between the present finite element solution and the analytical solution from MYERS *(1987) and* DAS *et al. (1991a) for radial temperature profiles in a finite cylinder at different longitudinal positions at 1000 s. Tau is the non-dimensional time given by diffusivity x time/radius*^{2}.

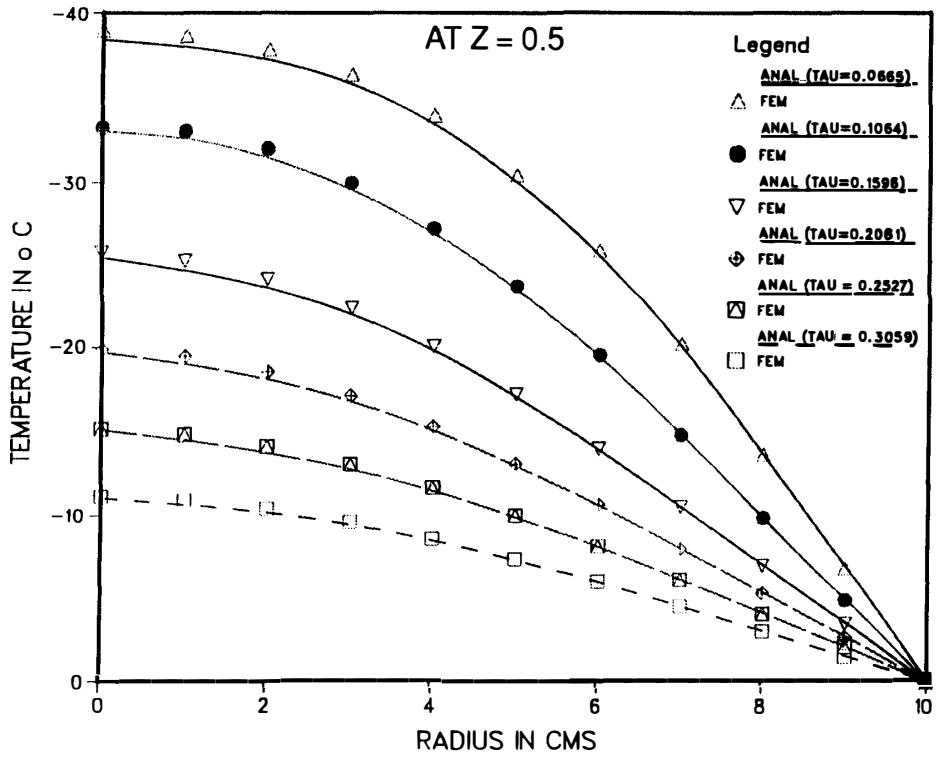

Fig. 8. (d) Comparison between the present finite element solution and the analytical solution from MYERS *(1987) and* DAS *et al. (1991a) for radial temperature profiles at mid-section of a finite cylinder at different time intervals.*

results obtainable through the series solution in DAS *et al.* (1991a) and MYERS (1987).

5.2. Freezing of boreholes

For the thermo-mechanical drill developed at PICO, one of the drilling fluids we are experimenting with is hot water. After the coring operation is complete, residual water is left in the boreholes. The same is the case for pure thermal drilling by a hot-water nozzle. Often the boreholes are kept open for a long period of time to conduct downhole experimentation. Therefore, an estimate of the freezing rate of these boreholes is a necessity.

The case considered here is for the inward radial freezing around a water hose of 3 cm diameter. The hose is placed in a borehole drilled in ice that has a diameter of 40 cm. The one-dimensional mesh with 30 elements and 32 nodes used to simulate the problem is shown in Fig. 9a. The temperature of the residual water in the borehole is 5°C (KOCI, 1984). The following thermal properties were taken as the input parameters from YEN *et al.* (1991). For the frozen zone, thermal conductivity K = 2.298 W/m·°C and the specific heat C = 2.100 kJ/kg·°C. For the thawed zone, thermal conductivity K = 0.5819 W/m·°C and the specific heat C = 4.186 kJ/kg·°C. Latent heat L = 305361 kJ/m^3, and the phase change temperature = 0°C. In Fig. 9a displaying the mesh, the inner radial boundary at the hose surface is maintained at 5°C and the outer radial boundary is –5°C. The top and bottom surfaces are considered insulated. Figure 9b shows temperature profiles at different time intervals.

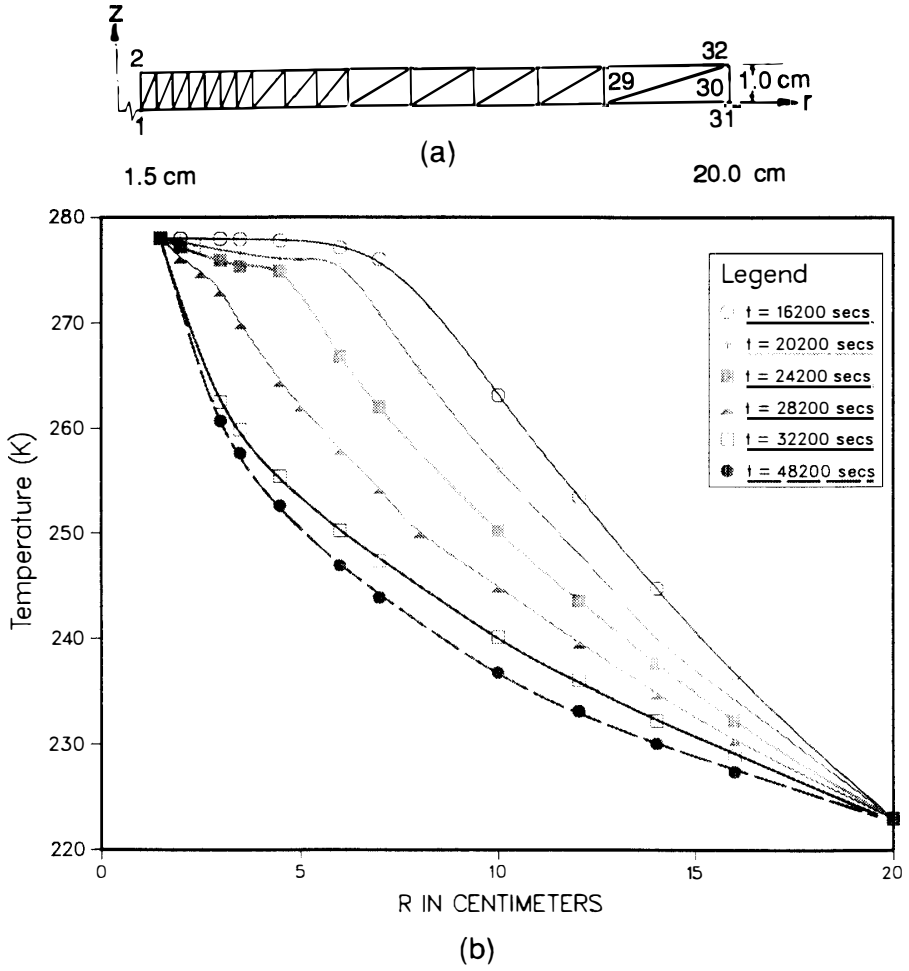

Fig. 9. (a) Mesh used for simulating the one-dimensional model of borehole freezing with a hose at the center. (b) Temperature profiles in the borehole during freezing at different time intervals for an ice temperature of −50°C

Next, we ran the program for different borehole wall temperatures. The borehole wall temperatures (*i.e.*, boundary condition at outer radial boundary) employed for this simulation are taken from HUMPHREY and ECHELMEYER (1990). As is evident from Fig. 9c showing the movement of the freeze front with time, the lower the temperature at the borehole wall, the less time it takes to refreeze.

The next case considers a large borehole (76 cm) made by hot-water drilling and is left water-filled with the hose removed. A one-dimensional mesh (Fig. 10a) with 76 elements and 78 nodes was used to simulate the inward radial freezing of this borehole with a radius of 38 cm (KOCI, 1984). The thermal properties used for simulating this problem are the same as those for the previous example. The centerline and the top and bottom surfaces were considered to be insulated. The outer boundary temperatures were assigned two different values. The program was run with two different borehole wall temperatures of 245 K (–28°C)and 256 K (–17°C) (KOCI, 1984). The progression of the freeze front at different time intervals is shown in Fig. 10b.

2-D Borehole Case: This case is for an axisymmetric freezing problem for the 70-cm borehole in *r-z* plane. The mesh used for simulating this case consisted of 506 elements

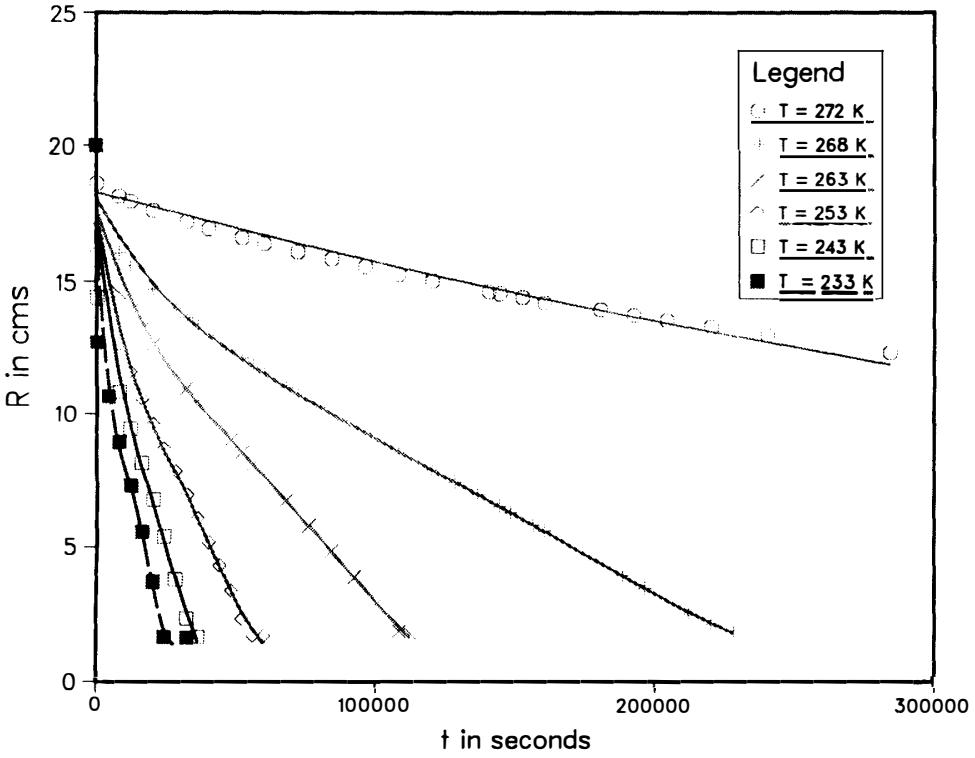

Fig. 9. (c) Locations of radii of freezing at different times within the borehole subjected to different wall temperatures from HUMPHREY *and* ECHELMEYER *(1990).*

and 288 nodes and is presented in Fig. 11a. The borehole radius is 20 cm and the hose radius is 1.5 cm; they are the same as one of the previous problems. The height of the borehole modeled is 100 cm. The top and the bottom boundary of the borehole in Fig. 11a are subjected to constant temperatures of −20°C and −50°C respectively, while the inner and the outer radius of the borehole are held at temperatures of 1.8°C and −40°C respectively (KOCI, personal communication, 1992). Initial temperature of water left in the borehole was 1.8°C. These temperatures can all be changed to suit field values and many cases can be run with this program. The migration of the phase change isotherm in this two-dimensional problem subjected to the specified boundary conditions is presented in Fig. 11b. Notice the progress of freezing until the time 46210 s (12.8 hr) when completion of freezing around the hose occurs. The time to finish freezing will change with other boundary and initial temperatures and can be explored easily by repetitively running the program.

5.3. Freezing of PICO ice test well

The PICO ice test well is shown in Fig. 12a. The inside radius of the well is about 50 cm. The mesh used for simulating this as a one-dimensional case consists of 24 elements and 26 nodes, as presented in Fig. 12b. The temperature of the water left in the well was assumed to be 1.66°C (35°F), which can be easily changed for other test runs. Boundary conditions for the finite element mesh of Fig. 12b are: the centerline and the top and bottom surfaces were considered to be insulated whereas the outer radial surface was assigned values(see Table 1) varying from −18°C (0°F) to −0.11°C (31.8°F) - the

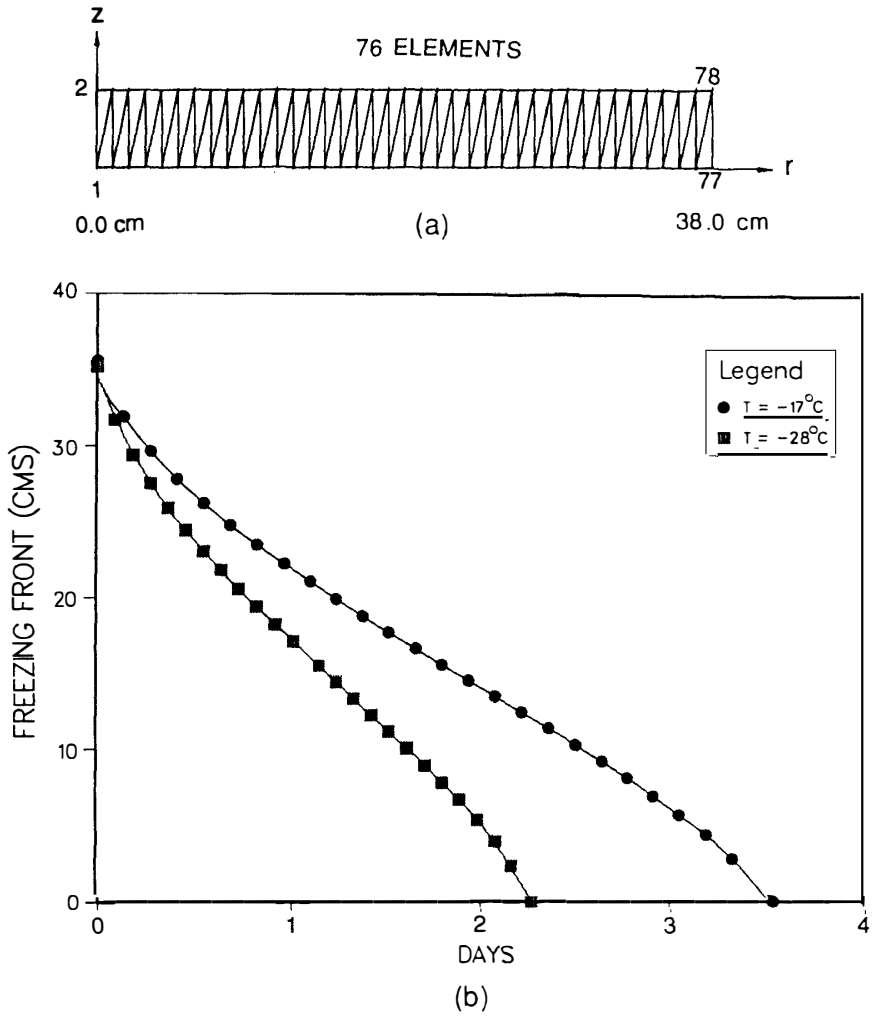

Fig. 10. (a) Mesh employed for simulation of borehole freezing with no hose. (b) Movement of freezeng front inside borehole with no hose for two different ice temperatures (KOCI, 1984).

temperature of the permafrost surrounding the well. The program was run for these different boundary temperatures (which can be attained through the cooling coil provided around the periphery of the well).

The freezing time required for complete closure of the well is shown in Table 1. Different time steps used in the computations were Δt = 40, 50, 100, 200, and 400 s without any perceptible change in the final results. Therefore, the program is stable and does not show unusual variations with different time steps. Finally, a time step Δt of 100 s was adopted to generate the freezing time given in Table 1. From this table we see natural freezing by the influence of permafrost will take 1.8 years. The closure rates are dependent on boundary temperatures and the initial water temperature.

2-D Test Well Simulation : This is a two-dimensional treatment of the same problem involving the ice test well in an *r-z* plane. The mesh consists of 460 elements and 264 nodes as shown in Fig. 13a. Half of the height of the well was simulated for illustration purposes so that we have less elements to compute. The water column in the well was

(a)

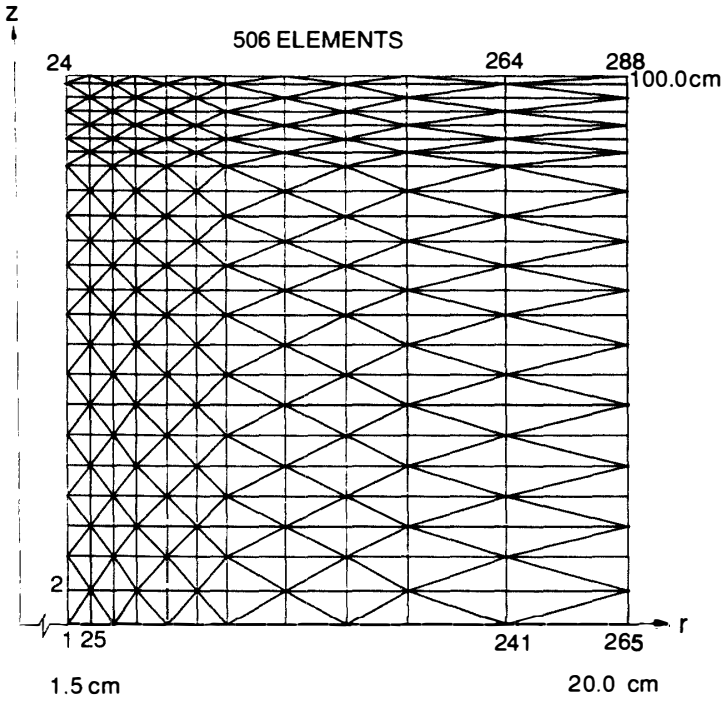

(b)

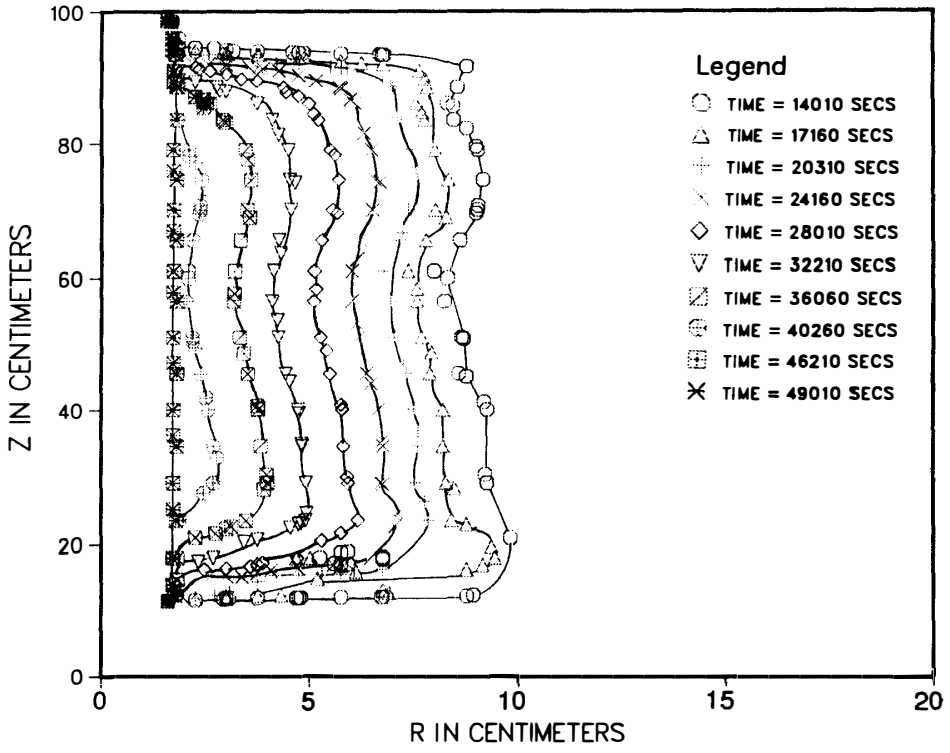

Fig.11. (a) Mesh used to simulate axisymmetric freezing of boreholes with a hose at the center. (b) Movement of freezing front with time in an r-z plane for borehole freezing.

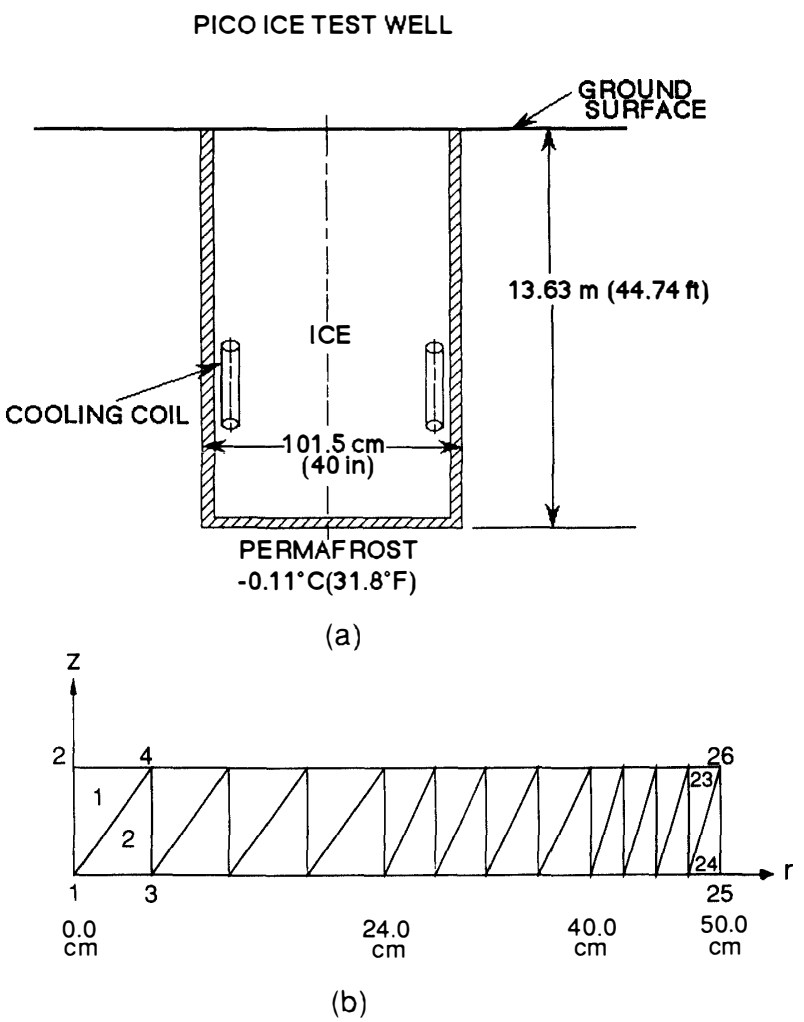

Fig.12. (a) Geometry of the PICO ice test well.
(b) Mesh employed to simulate freezing of the ice test well.

Table 1. Time taken for complete freezing of the PICO ice test well.

Boundary temperature	Time in days
−18°C (0°F)	6
−12°C (10°F)	8.5
−7°C (20°F)	15.3
−4°C (25°F)	25.8
−1°C (30°F)	88.4
−0.11°C (31.8 °F) (permafrost)	660

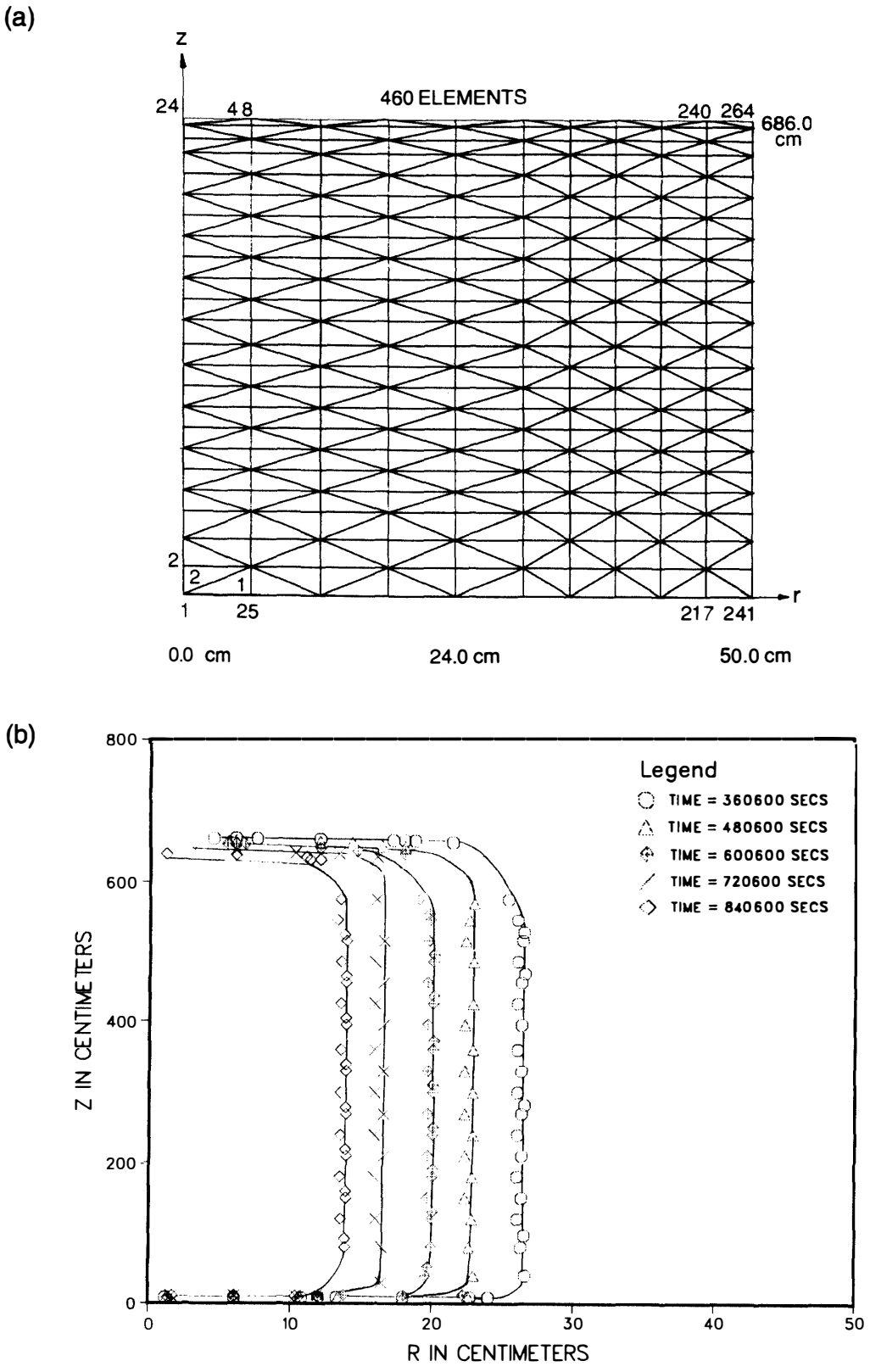

Fig. 13. (a) Mesh employed for simulating freezing of the ice test well for an axisymmetric simulation. (b) Migration of the phase change isotherm with time in an r-z plane for freezing of the ice test well.

assumed to be 6.86 m (22.5 feet) high. The boundary conditions at the top, the bottom, and the outer surfaces of the modeling zone in Fig. 13a are subjected to temperatures of –7°C (20°F) (cold air), –0.11°C (permafrost), and –7°C (20°F) (cooling coil), respectively. The centerline of the domain in Fig. 13a conforms to insulated condition due to symmetry. The progression of the phase change isotherm as time progresses is illustrated in Fig. 13b, representing the right side as the frozen zone and the left side as the unfrozen zone.

6. Conclusions

A finite element algorithm for solving heat conduction problems with phase change in a cylindrical (*r-z*) coordinate system was developed and implemented in the finite element code FEMRZ. The inclusion of phase change ability was accomplished by using the Dirac delta function to simulate effective heat capacity. Validation of the method at various stages of its evolution showed good performance. Six test cases of steady and unsteady heat conduction with and without phase change demonstrated accuracy of the results produced by this program. The program was then applied to ice drilling problems to predict temperature profiles in ice cores and the freeze-up of boreholes and the PICO ice test well.

References

DAS, D. K. and SRIVASTAVA, V. (1991) : Application of a finite element model to hydrate reservoirs. Proc. 3rd Int. Symposium on Cold Regions Heat Transfer, ed. by J. P. ZARLING, and S. L. FAUSSETT. Fairbanks, Unibersity of Alaska Fairbanks, 83–98.

DAS, D. K., JOIS, S. S. and KELLEY, J. J. (1991a) : Analytical solutions for determining ice core temperatures. Mechanical Engineering News, **28** (3), 9–13.

DAS, D. K., JOIS, S. S., GOERING, D. J. and KOCI, B. R. (1991b) : Analytical solution for temperature distribution in ice cores. Polar Ice Coring Office Report No. TR-91-3. Fairbanks, University of Alaska Fairbanks, 28 p.

DAS, D. K., KOCI, B. and KELLEY, J. J. (1992) : Development of a thermal mechanical drill for sampling ice and rock from great depths. Tunnelling Underground Space Technol., **7**, 377–382.

GOERING, D. (1984) : Unsteady-state heat conduction by the finite element method. M. S. thesis, University of Alaska Fairbanks, Alaska.

HUEBNER, K. H. and THORNTON, E. A. (1982) : The Finite Element Method for Engineers, 2nd ed. New York, J. Wiley, 215–218, 418–420, 498–500.

HUMPHREY, N. and ECHELMEYER, K. (1990) : Hot-water drilling and borehole closure in cold ice. J. Glaciol., **36,** 287–298.

JOIS, S. S. (1992) : Finite element approach for determining temperature variation in ice cores. M. S. thesis, University of Alaska Fairbanks, Alaska.

KOCI, B. R. (1984) : Ice drilling technology. CRREL Spec. Rep., **84-34**, 101–103.

KRIETH, F. and BOHN, M. (1986) : Principles of Heat Transfer. 4th ed. New York, Harper and Row Publ., 124–127.

LUNARDINI, V. J. (1981) : Heat Transfer in Cold Climates. New York, Van Nostrand Reinhold, 432–449.

MYERS, G. E. (1987) : Analytical Methods in Conduction Heat Transfer. New York, Genium Publ., 139–142.

O'NEILL, K. (1983a) : Fixed mesh finite element solution for Cartesian two-dimensional phase change. ASME J. Energy Resouroes Technol., **105**, 436–441.

O'NEILL, K. (1983b) : Solution of two-dimensional axisymmetric phase change problems on a fixed mesh, with zero width phase change zone. Proc. 3rd Int. Conf. on Numerical Methods in Thermal Problems. Seattle, Washington, 134–146.

RAO, S. S. (1989) : The Finite Element Method in Engineering. New York, Pergamon Press, 491–495.

REDDY, J. N. (1984) : An Introduction to the Finite Element Method. New York, McGraw Hill, 194–206, 231–233, 299–304, 424–437.

SRIVASTAVA, V. (1988) : Finite element solution of a cylindrical phase change problem and its application to dissociation of gas hydrates. M. S. thesis, University of Alaska Fairbanks, Fairbanks, Alaska.

SQUARE, W. (1970) : Integration for Engineers and Scientists. New York, Elsevier, 184–185.

WHITE, F. M. (1984) : Heat Transfer. Massachusetts, Addison-Wesley Publ., 221–222.

YEN, Y.-C., CHENG, K. C. and FUKUSAKO, S. (1991) : Review of intrinsic thermophysical properties of snow, ice, sea ice and frost. Proc. 3rd Int. Symposium on Cold Regions Heat Transfer, ed. by J. P. ZARLING, and S. L. FAUSSETT. Fairbanks, University of Alaska Fairbanks,187–218.

(Received April 20, 1993)

Nomenclature

A_e	area of the element
A_f	frozen element area
A_t	thawed element area
C	volumetric heat capacity = ρC_p, J/m^3 ·°C
C_p	specific heat, J/kg ·°C
C_{eff}	effective volumetric heat capacity
C_{eq}	equivalent volumetric heat capacity
C_f	volumetric heat capacity of frozen material
C_t	volumetric heat capacity of thawed material
ρ	density, kg/m^3
g	heat source/sink in the system, W/m^3
h	convective coefficient, W/m^2·°C
K_{eq}	equivalent thermal conductivity, W/m·°C
K_f	thermal conductivity of frozen material
K_r	thermal conductivity in r - direction
K_t	thermal conductivity of thawed material
K_z	thermal conductivity in z - direction
L	latent heat, J/m^3
l	length of linear isotherm within the element
l_{ij}	length of the i-j side of a triangular element
$\hat{q}$	prescribed heat flux at boundaries, W/m^2
r_i, z_i	coordinates of the i^{th} node of an element
$\bar{r},\bar{z}$	coordinates of the centroid of an element
t	time
T	variable temperature
T_i	initial temperature
T_o	phase change temperature
T_∞	ambient temperature
$\hat{T}$	prescribed temperature at boundaries
v	test function
$[H]$	convective term matrix
$[K_k]$	conductivity matrix
$[M]$	heat capacitance matrix

$\{F_c\}\{F_q\}\{F_g\}$	convective, heat flux, and heat source/sink vectors, respectively
α, β, γ	coefficients of shape function
$\Gamma^{(e)}$	boundary of an element
δ	Dirac-delta function
Ψ_i, Ψ_j	shape functions
Ψ_{ia}, Ψ_{ja}	value of shape function evaluated at point a
Ψ_{ib}, Ψ_{jb}	value of shape function evaluated at point b
$\Omega^{(e)}$	domain of an element